Squeezing (ATS) scheme, **CERN-ATS-2012-069**, pp.128-134, Chamonix 2012 Workshop on LHC Performance, Chamonix, France, 6 - 10 Feb 2012.

20. S. Fartoukh, *et al*., *The 10 cm beta* ATS MD*, **CERN-ATS-Note-2013-004 MD**, CERN, Geneva, Switzerland, 2013.

21. R. de Maria, S. Fartoukh, *SLHCV3.0: layout, optics and long term stability*, **SLHC-Project-Report 50**, CERN, Geneva, Switzerland, 2010.

4.3 Novel Lattice Solutions for the LheC

S.A. Bogacz[2], O. Brüning [1], E. Cruz-Alaniz[3], A. Latina[1], D. Pellegrini[1], D. Schulte[1], R. Tomás [1], A. Valloni[1,3]

[1]CERN, [2]Jefferson Lab, [3]University of Liverpool

bogacz@jlab.org

4.3.1 Introduction

Unprecedently high luminosity of 10^{34} $cm^{-2}s^{-1}$, promised by the LHeC accelerator complex poses several beam dynamics and lattice design challenges. As part of accelerator design process, exploration of innovative beam dynamics solutions and their lattice implementations is the key to mitigating performance limitations due to fundamental beam phenomena, such as: synchrotron radiation and collective instabilities. This article will present beam dynamics driven approach to accelerator design, which in particular, addresses emittance dilution due to quantum excitations and beam breakup instability in a large scale, multi-pass Energy Recovery Linac (ERL). The use of ERL accelerator technology to provide improved beam quality and higher brightness continues to be the subject of active community interest and active accelerator development of future Electron Ion Colliders (EIC). Here, we employ current state of though for ERLs aiming at the energy frontier EIC. We will follow conceptual design options recently identified for the LHeC. The main thrust of these studies was to enhance the collider performance, while limiting overall power consumption through exploring interplay between emittance preservation and efficiencies promised by the ERL technology. This combined with a unique design of the Interaction Region (IR) optics gives the impression that luminosity of 10^{34} $cm^{-2}s^{-1}$ is indeed feasible.

4.3.2 Challenges of 60 GeV ERL

4.3.2.1 *Principles and Design Considerations for High Energy ERLs*

Energy Recovery Linacs accelerate electron bunches of linac quality, and then recover beam energy (after the collision) by deceleration through the same linac, before dumping the bunches at low (injection) energy. Energy recovery has the benefits of supporting high beam energy and power while maintaining high beam quality, including

small beam sizes as delivered by linacs; minimizing activation by dumping low-energy (and thus low-power) beam; and ensuring power efficient accelerator operation.

An ERL would also allow for more ‘disruptive’ applications than the ones that would be tolerable by a ring and can achieve a smaller machine footprint. However, there is a ‘payback’ in terms of increased complexity, which exceed the ones for both rings and linacs.

Both the acceleration and deceleration can take place simultaneously in the same RF cavities, typically with interleaved bunches, which minimizes the fluctuations of the power stored in the cavities. This scheme requires both the accelerating and decelerating beam to travel in the same direction; therefore a recirculating arc is necessary to connect the two ends of the linac. Eventually, the machine can be arranged in a racetrack configuration with a second linac in the opposite straight section.

In order to reach higher energies, multi-turn recirculation can be adopted, with more passages on the accelerating and on the decelerating phases. A number of bunches at different energies will then coexist in the machine, requiring optics solutions capable of accommodating all of them. The choice of the number of recirculating passes and the machine size (linac length and arc radius) is driven by the desired energy, with constraints mostly coming from the impact of synchrotron radiation. In general, one can estimate the arc radius by fixing the maximum energy loss in the highest energy arc, according to beam quality issues and power considerations. The total number of passes at lower energies should then be limited by similar considerations. This allows one to fix the required voltage in the linac and therefore the machine size. Due to the scaling of the radiation effects, high energy designs tend to converge towards very small pass numbers and powerful linacs, while lower energy ones can afford to bend the beam in many passes.

These considerations might not apply if the machine is to be installed into an existing tunnel, which may pose other constraints. However, since the current in the linac scales with the number of turns, one may still want to limit these in order to allow for higher beam currents without incurring in instabilities caused, for instance, by long range wakefields and the ion/electron cloud.

The material presented in the following sections is adapted from [1,2,3], where more details and in-depth explanations can be found. The lattice solutions have been tested with extensive beam dynamic simulations.

4.3.2.2 *Layout of the LHeC*

The ERL design for the LHeC electron facility is sketched in Fig. 1. The machine is arranged in a racetrack configuration hosting two superconducting linacs in the parallel straights and three recirculating arcs on each side. The linacs are 1 km long and the arcs have 1 km radius, additional space is taken up by utilities like spreading, matching and compensating sections. The total length is 9 km: 1/3 of the LHC circumference.

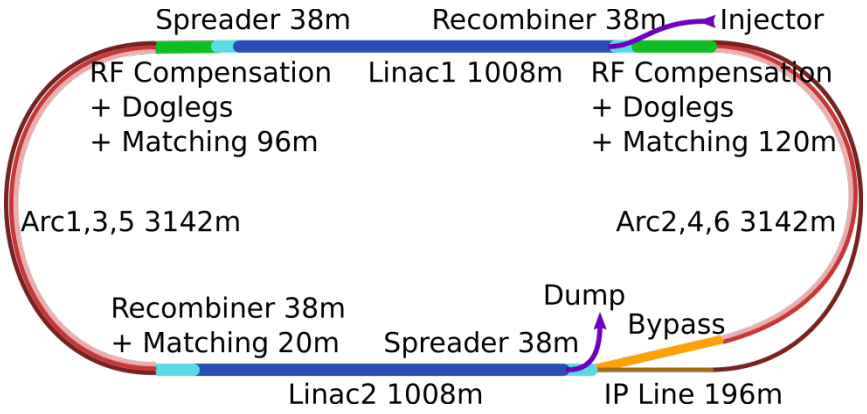

Figure 1: Scheme of the LHeC ERL layout.

Each of the two linacs provides 10 GV accelerating field, therefore a 60 GeV energy is achieved in three turns. After the collision with the protons in the LHC, the beam is decelerated in the three subsequent turns. The injection and dump energy has been chosen at 500 MeV.

4.3.2.3 *Linac Design and Optimization*

Each 1 km long linac hosts 72 cryomodules, each containing 8 cavities for a total of 576 cavities per linac operating at 802 MHz. In the baseline design a quadrupole is placed every two cryomodules providing a FODO configuration. Note that the optics of a high gradient linac can be substantially perturbed by the additional focusing coming from the RF [4]. It is therefore important to make sure that it is properly modelled.

Energy recovery in a racetrack topology explicitly requires that both the accelerating and decelerating beams share the individual return arcs. This in turn, imposes specific requirements for TWISS function at the linacs ends: the TWISS functions have to be identical for both the accelerating and decelerating linac passes converging to the same energy and therefore entering the same arc.

To visualize beta functions for multiple accelerating and decelerating passes through a given linac, it is convenient to reverse the linac direction for all decelerating passes and string them together with the interleaved accelerating passes, as illustrated in Fig. 2. This way, the corresponding accelerating and decelerating passes are joined together at the arcs entrance/exit. Therefore, the matching conditions are automatically built into the resulting multi-pass linac beamline.

The optics of the two linacs are symmetric, the first being matched to the first accelerating passage and the second to the last decelerating one. In order to maximize the BBU threshold current, the optics is tuned so that the integral:

$\langle \beta E \rangle = \int \text{Acceleration } \beta/E \, ds$

is minimized. The resulting phase advance per cell is close to 130°. Non-linear strength profiles and more refined merit functions were tested, but they only brought negligible improvements.

More consistent improvements were obtained doubling the number of quadrupoles in the linacs (placing one every cryomodule) as show in Fig. 2. This has two benefits: enhances the BBU threshold and contains the beam sizes; which can possibly result in a smaller injection and dump energy.

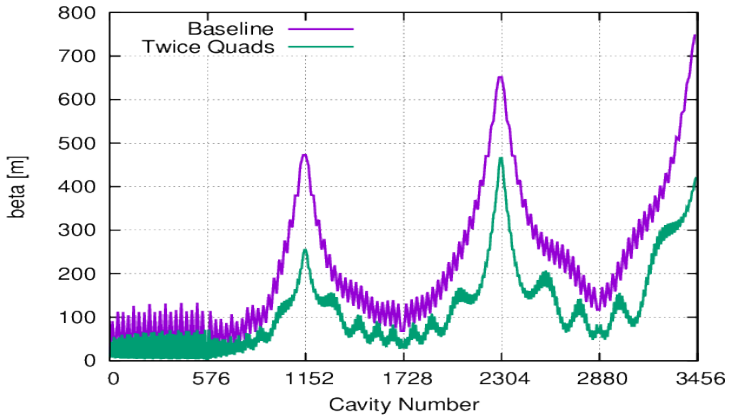

Figure 2: Beta function in the optimized LHeC Linacs during the acceleration. The linac contains 576 cavities. Only the first passage is well matched, the beams at higher energies need to be re-matched in dedicated sections (not shown here).

4.3.2.4 *Recirculating Arcs*

All six arcs (three on each side) are accommodated in a tunnel of 1 km radius. Their lattice cell adopts a flexible momentum compaction layout that presents the very same footprint for each arc. This allows us to stack magnets on top of each other or to combine them in a single design. The dipole filling factor of the cell is 76%; therefore, the effective bending radius is 760 m.

The tuning of each arc takes into account the impact of synchrotron radiation at different energies. At the highest energy, it is crucial to minimize the emittance dilution; therefore, the cells are tuned to minimize the dispersion in the bending sections, as in a theoretical minimum emittance lattice. At the lowest energy, it is possible to compensate for the bunch elongation with a negative momentum compaction setup which, additionally, contains the beam size. The intermediate energy arcs are tuned to a double bend achromat (DBA)-like lattice, offering a compromise between isochronicity and emittance dilution. Fig. 3 illustrates all three settings of the arc cells. Tapering will be required in particular for arc6, where the beam loses more than 1% of its total energy.

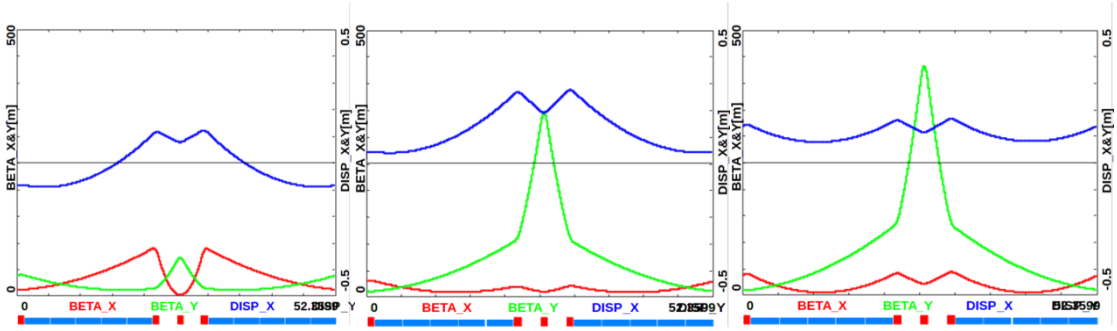

Figure 3: Different tunings of the arc cells at different energies. From left to right: low energy negative momentum compaction, middle energy DBA-like, high energy TME-like.

Before and after each arc a matching section adjusts the optics from and to the linac. Adjacent to these, additional cells additional cells are placed, hosting the RF compensating sections. The compensation makes use of a second harmonic field to replenish the energy lost by synchrotron radiation for both the accelerating and the decelerating beam, therefore allowing them to have the same energy at the entrance of each arc.

Path length-adjusting chicanes were also foreseen to tune the beam time of flight in order to hit the proper phase at each linac injection. Later investigations proved them to be effective only with the lowest energy beam, as these chicanes triggers unbearable energy losses if applied to the higher energy beams. A possible solution may consist in distributing the perturbation along the whole arc with small orbit excitations.

An alternative design based on FFAG have been proposed and explored. It allows one to transport multiple energies in the same beam pipe, although only a very specific energy is bent with a constant radius. A drop-in FFAG arc tuned to the 60 GeV energy showed promising results when substituted in the lattice, mainly because of the much higher bending filling factor, which mitigates synchrotron radiation. Nevertheless the LHeC would still need at least two FFAG arcs on each side and it is not yet clear if the benefits compensate for the added complexity.

4.3.2.5 *Spreaders and Recombiners*

The spreaders are placed after each linac, and they separate the bunches at different energies in order to route them to the corresponding arcs. The recombiners do just the opposite, merging the beams into the same trajectory before entering the next linac.

The spreader design consists of a vertical bending magnet, common for all beams, that initiates the separation. The highest energy, at the bottom, is brought back to the horizontal plane with a chicane. The lower energies are captured with a two-step vertical bending adapted from the CEBAF design [5]. This two-step design simplifies the suppression of vertical dispersion; however, it induces a non-negligible energy loss, especially for arc4, and also it drives the horizontal β function to very high values.

In order to mitigate this, a single-step design was developed. It employs seven quadrupoles to control the dispersion between the two bending dipoles. The energy loss

is reduced by factor of 5, and at the same time both the dispersion and the ***β*** functions are reduced. To avoid magnet interference, the quadrupoles of the two beam lines were appropriately shifted longitudinally. The maximum quadrupole gradient of 80 T/m will probably require superconducting magnet technology, however the cryogenics is readily available from the nearby linacs.

A comparison of the two designs for the arc2 spreader is shown in Fig. 4. Both of them provide a final vertical separation of ~0.5 m between the three arcs.

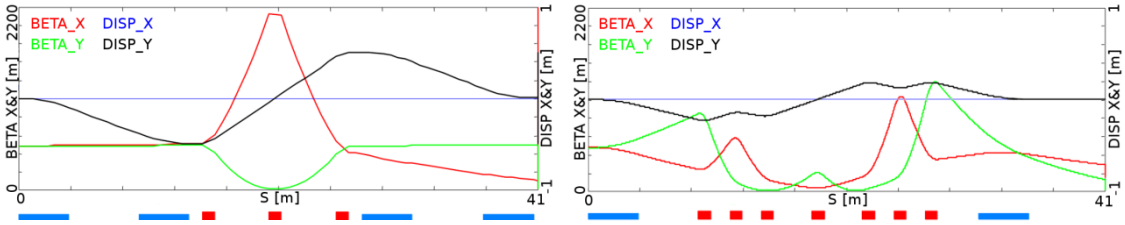

Figure 4: Comparison between the two spreader designs. Left: the CEBAF-like one, in two steps and Right: the single step developed to mitigate synchrotron radiation.

4.3.2.6 *The Bypass*

While after the last spreader the 60 GeV beam can go straight to the interaction region, the lower energies beams, at 20 and 40 GeV, needs to be further separated in order to avoid interference with the detector. Different design options for the bypass section were explored and the one that minimizes the extra bending has been chosen and installed in the lattice.

Ten arc-like dipoles are placed very close to the spreader, to provide an initial bending, which results in 10 m separation from the detector located 150 m downstream. The straight section of the bypass is approximately 300 m long. In order to join the footprint of arc6, 10 of the 60 standard cells in arc2 and arc4 are replaced with seven higher field cells. The number of junction cells is a compromise between the field strength increase and the length of additional bypass tunnel, as can be inferred from the scheme in Fig. 5.

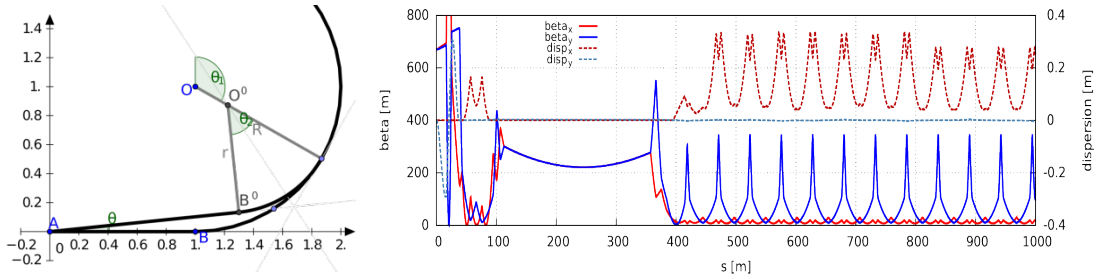

Figure 5: Layout of the bypass and Twiss along the line. One can recognize: the matching section from the linac, the initial bending, the long straight, the dispersion suppressor, seven cells with higher bending field and four regular arc cells.

The stronger bending in the junction cells creates a small mismatch which is corrected by adjusting the strengths of the quadrupoles in the last junction cell and in the first regular cell.

4.3.3 Interaction Region Optics: Integration into the HL-LHC ATS Optics

4.3.3.1 Nominal Design

The design of the LHeC interaction region (IR) aims at focusing the counter-clockwise rotating proton Beam2 colliding it with the electron beam of the ERL while the clockwise proton Beam1 bypasses the interaction.

A first conceptual design of the LHeC Linac-Ring IR was discussed in [6]. The aim of this design was to achieve head-on electron-proton collisions in the interaction region at a luminosity $L = 10^{33}$ $cm^{-2}s^{-1}$, requiring a low β^* (β function at the interaction point) of 10 cm. This low β^* was achieved by implementing a new inner triplet (IT) of quadrupoles which was positioned as close as possible to the interaction point (IP) to reduce chromaticity.

An illustration of the three beams passing through the inner triplet is shown in Fig. 6. The closest quadrupole to the IP (Q1) is based on a half aperture design to minimize the synchrotron radiation produced by the electron beam. A new type of magnet has been proposed for the Q1 to overcome some of the present challenges of the design [7].

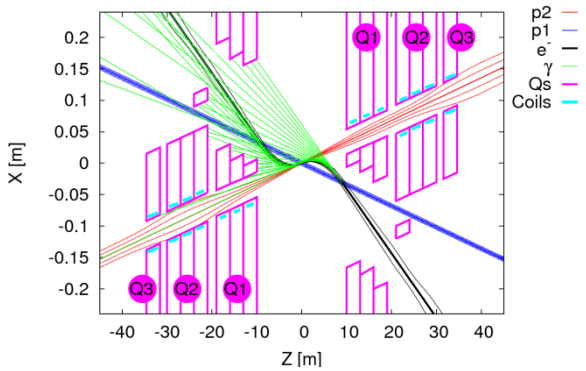

Figure 6: Focussed proton Beam2 (red) colliding with electron beam (black) while the unfocussed proton Beam1 bypasses the interaction. Each proton and electron beam passes through its corresponding aperture in the inner triplet.

It was initially hoped that a compact Nb_3Sn triplet at a distance (L^*) of 10 m from the interaction point would allow the use of a conventional scheme for chromaticity correction using the arc sextupoles. However, after matching the new triplet to the LHC and correcting the chromaticity the chromatic beta beating at $dp/p = \pm 0.001$ is about 100%, which is not tolerable regarding collimation and machine protection issues [6].

The challenge consists in developing an optics that not only achieves the β^* of 10 cm while leaving the HL-LHC insertions undisturbed but that also provides a dedicated chromaticity correction scheme.

4.3.3.2 Implementation of the LHeC into the ATS scheme

The Achromatic Telescopic Squeezing scheme is a novel technique proposed for the HL-LHC project in IR1 and IR5 (ATLAS and CMS respectively) to reduce the β*, overcoming the limitations of the optics given by the quadrupole strengths in the IR's and the chromatic correction efficiency limits [8].

The ATS consists of creating and absorbing a β-beating wave in the arcs adjacent to the low β insertions. By adjusting the phase advance in the arc cell to π/2, this β-beating wave is carefully constructed in a way that will increase the β function at the location of every alternate sextupole in the arcs, and consequently increase its efficiency for chromatic correction, at the same rate than the β* gets reduced.

Although reducing β* increases the IR chromaticity, the improvement in sextupole efficiency in the arcs leads to a net benefit.

Following a proposal to integrate the LHeC IR into the HL-LHC lattice using the ATS scheme [9], a first study of the required proton optics for the nominal case was presented in [10]. This procedure involved extending the β-beating wave in the arc between IR2 and IR3 by adjusting the arc cells in sector 23 to the phase advance of π/2 and imposing the ATS matching conditions for proton beam 2 for the left and right phase advance of IR2 (with respect to IP2) resulting in a β* of 10 cm in IR2 for the LHeC and a β* of 15 cm in IR1 and IR5 for the HL-LHC. The β functions along the LHC with this optics are shown in Fig. 7.

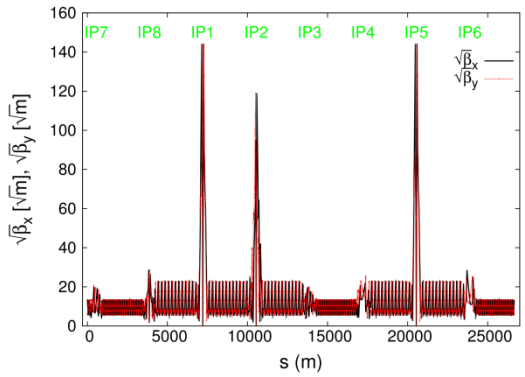

Figure 7: LHeC ATS collision optics for beam 2 with $\beta^* = 10$ cm and $L^* = 10$ m in IP2 and $\beta^* = 15$ cm in IP1 and IP5.

4.3.3.3 Flexibility of the design

The flexibility of the design described above (based on the ATS scheme) is of great interest because of the benefits that could be obtained in terms of synchrotron radiation power and luminosity.

Two methods were used to assess the flexibility. First β^* is reduced as far as possible, to determine the maximum luminosity that can be achieved. Second, L^* is increased as far as possible, to reduce the synchrotron radiation power from the electron beam: with larger L^*, less bending is required to guide the electron beam into the field-free aperture

of the proton inner triplet. This is illustrated in Fig. 8, where the synchrotron radiation power is given as a function of L* with a β^* of 10 cm.

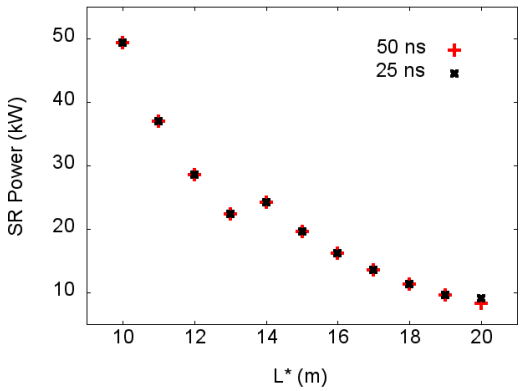

Figure 8: Synchrotron radiation power as a function of L*. The black and red symbols (almost overlaid in the image) show the synchrotron radiation for the minimum beam separation for bunch spacing of 25 ns and 50 ns respectively, and both for the case of the CDR luminosity of $L = 10^{33}$ $cm^{-2}s^{-1}$.

Keeping the optics parameters at either end of IR2 fixed, the strengths of the quadrupoles in the IR2 can be used as variables to find solutions for different values of β^* and L^*.

Stable solutions for optical designs with L^* between 10 m and 20 m and β^* fixed at 10 cm have been found, as well as the cases with $\beta^* = \{5, 6, 7, 8, 9, 10, 20\}$ cm and L^* fixed at 10 m [11].

4.3.3.4 *Chromaticity Correction*

The chromaticity correction for the HL-LHC case was achieved using only one family of sextupoles at each side of the IPs. However, in the LHeC, an imbalance exists due to the β wave produced to perform the telescopic squeeze in both IP1 and IP2. The path to follow is then trying to achieve a global correction that might break the locality of the chromatic correction but that will certainly bring benefits in terms of controlling the chromatic aberrations.

The strengths of all sextupole families are varied to fix the horizontal and vertical chromaticities to values $Q'_x = Q'_y = 2$, and to reduce the chromatic betatron amplitude functions in the collimation insertions IR3 and IR7 to $W_x, W_y < 200$.

Chromatic correction including control of the tune spread to avoid resonances up to order 9 was achieved for a minimum β^* of 8 cm with $L^* = 10$ m, and a maximum L^* of 18 m with $\beta^* = 10$ cm.

The natural chromaticity for the different optical designs in terms of L^* and β^* along with the limit of the chromatic correction is shown in Fig. 9.

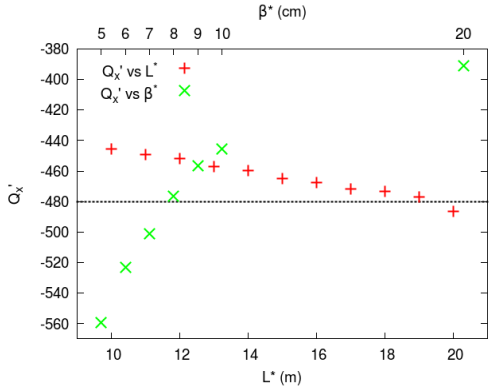

Figure 9: Limit of the chromatic correction (black dashed line) overlaid in the plot Qx' vs L* (red) and Qx' vs β*(green).

4.3.3.5 *Tracking studies*

Dynamic Aperture (DA) studies were performed to study the impact of the different lattices on long term stability of the beam. The DA calculations were carried out in SixTrack[1] over 10^5 turns and considering 60 different realizations (seeds) of the LHC magnet errors. So far, the errors of the new IT and recombination dipoles D1 and D2 for IR1, IR2 and IR5 have not been included, as well as the errors for the additional quadrupoles Q4, Q5 for the HL insertions IR1 and IR5.

Figure 10 shows the minimum dynamic aperture for all sees and angles as a function of L^* with β^* fixed at 10 cm. A small reduction of DA is observed for the case $L^* = 15$ m but it is still very close to the DA found for $L^* = 10$ m. However, for $L^* > 15$ m the higher β functions reached in the location of the inner triplet causes aperture losses and therefore a significant reduction of DA.

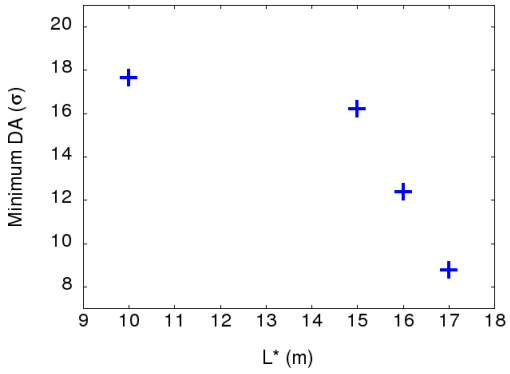

Figure 10: Minimum dynamic aperture over 60 seeds and 5 angles as a function of L^* for LHeC lattices with collision optics ($\beta^* = 15$ cm at IP1 and IP5, $\beta^* = 10$ cm at IP2) over 10^5 turns. Cases with L* = 10 m, 15 m, 16 m and 17 m are shown.

[1] http://sixtrack.web.cern.ch/SixTrack

Figure 11 shows the minimum dynamic aperture for all seeds and angles now as a function of β^* all with L^* fixed at 10 m. Results show a reduction in dynamic aperture for cases with $\beta^* < 10$ cm, with similar results between the cases with $\beta^* = 8$ and $\beta^* = 9$ cm, but a clear reduction for the case with $\beta^* = 5$ cm.

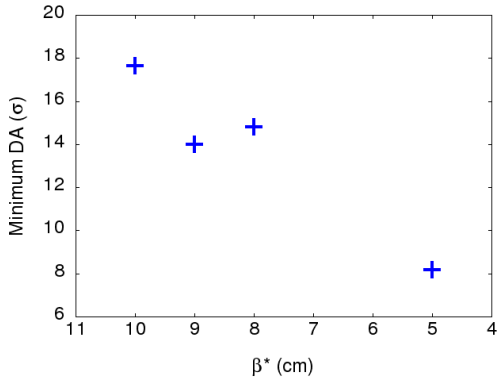

Figure 11: Minimum dynamic aperture over 60 seeds and 5 angles as a function of β^* for LHeC lattices over 10^5 turns. Cases with $\beta^* = 5$ cm, 8 cm, 9 cm and 10 cm (all with L* = 10m) are shown.

In summary, we have demonstrated the feasibility of integrating the LHeC into the HL-LHC by extending the ATS scheme. For the CDR luminosity of $L = 10^{33}$ $cm^{-2}s^{-1}$ studies show the possibility of increasing L* up to 15 m, bringing benefits in terms of the synchrotron radiation power and magnet design. On the other hand the upgraded luminosity of 10^{34} $cm^{-2}s^{-1}$ is within reach but further studies are required to produce a feasible design.

4.3.4 PERLE a Proposed ERL Test Facility at CERN

4.3.4.1 *Design Concept and Parameters*

PERLE stands for Powerful Energy Recovery Linac Experiment [16]. The test facility aims at a 1 GeV beam energy, which can be achieved in a recirculating SC linear accelerator operating with high currents in multi-pass (3) energy recovery mode. Independently, it could be used for variety of physics applications

PERLE is envisioned as a staged project. The final baseline design (**Error! Reference source not found.**2) would consist of the following basic elements:

- A 5 MeV injector;
- Two 150 MeV linacs consisting of eight 5-cell SC structures;
- Optics transport lines including spreader regions at the exit of each linac to separate and direct the beams via vertical bending, and recombiner sections to merge the beams and to match them for acceleration through the next linac;
- Beam dump at 5 MeV.

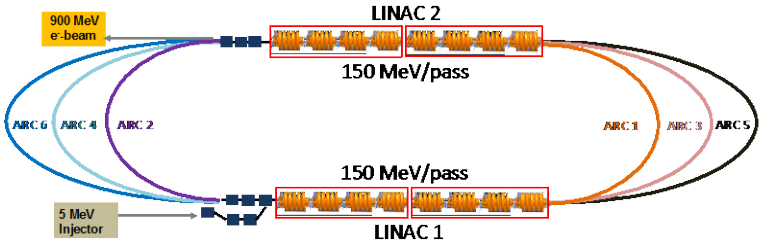

Figure 12: ERL accelerator complex of two parallel linacs consisting of two 4-cavity cryomodules each achieving 150 MeV acceleration per linac (300 MeV per pass).

Each beam recirculates up to three times through both linacs to boost the energy to about 900 MeV. To enable operation in the energy recovery mode after acceleration the beam is phase shifted by 180° and then sent back through the recirculating linac at a decelerating RF phase. The set of main parameters incorporated into the ERL prototype is shown in Table 1.

The first phase of the staged construction would only use two 4-cavity cryomodules and a single pass – it could reach 150 MeV and be used for injector studies and SC RF tests. A subsequent upgrade would involve installation of two additional arcs on each side to raise the beam energy up to 450 MeV. This configuration accommodates additional space available for implementation of feedback, phase-space manipulations, and beam diagnostic instrumentation. In phase 3, four additional cavities in each linac are added to permit energy recovery recirculation tests at full energy.

Table 1: Basic Parameters of PERLE

TARGET PARAMETER	**VALUE**
Injection Energy	5 MeV
Maximum Energy	900 MeV
Normalized Emittance $\gamma\varepsilon_{xy}$	< 25 mm mrad
Average Beam Current	> 12.8 mA
Beam charge	320 pC
Bunch Spacing	25 ns
RF frequency	801.58 MHz
Duty Factor	CW

4.3.4.2 *Injector*

The injector of the ERL test facility needs to deliver beams with an average current of 12.8 mA (with possibility of future upgrades to deliver polarized electrons or larger currents) and the energy of ~ 5 MeV. Bunches with a charge of 320 pC or higher follow with a repetition rate of 40.1 MHz (20^{th} sub-harmonic of 801.58 MHz). There are

several possibilities to meet these specifications. One option is to use a grid modulated thermionic gun followed by a multi stage bunching-accelerating structure. This choice however will rule out any future upgrade to deliver polarized electrons. Photocathode guns where electrons are emitted from the photocathode illuminated with laser light are more flexible in terms of the beam charge and temporal structure and allow operation with both polarized and un-polarized photocathodes. Presently, only DC technology may be considered as mature and applicable to an ERL test facility.

To deliver beams with the parameters required for PERLE, preliminary simulations indicate the possibility of using a 350 kV DC gun operating with a Cs_3Sb photocathode. An optimal beam emittance of 2π·mm·mrad can be obtained with a laser pulse with hat top spatial distribution with a diameter of 3 mm and a flat top 80ps laser pulse. The RMS bunch length at 1 m from the photocathode is 8.5 mm (36 ps) and depends only slightly on the laser pulse length.

Once emerged from the gun, an energy chirp should be introduced to longitudinally compress the bunch and compensate the bunch elongation due to the space charge repulsion (typically done with an RF buncher). In order to provide linear energy modulation the frequency of the buncher should be selected to have a bunch flight time at the buncher shorter than 10° of its RF phase. At 320 pC and rms buncher flight time of 36 ps the required frequency should be less than 775 MHz. Practically attractive is 400.8 MHz - the first sub-harmonic of the ERL frequency. Gradual beam compression and acceleration can be provided with a booster consisting of a series of single cell 801.58 MHz cavities with individual coupling and control of amplitude and RF phase.

4.3.4.3 *Transport Optics*

Appropriate recirculation optics is of fundamental concern in a multi-pass machine to preserve beam quality. The design consists of three different regions, the linac optics, the recirculation optics and the merger optics. A concise representation of multi-pass linac optics is illustrated in Fig. 13.

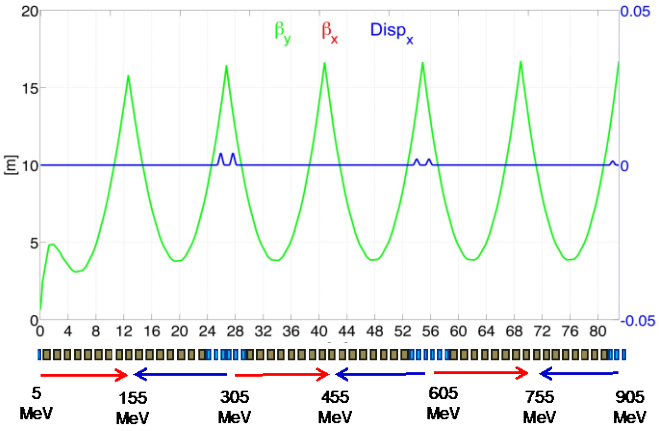

Figure 13: ERL multi-pass linac optics. The requirement of energy recovery puts a constraint on the exit/entrance Twiss functions for the two linacs. Green and blue curves show, respectively, the evolution of the beta functions amplitude and the horizontal dispersion for Linac 1. Red and blue arrows indicate the passages of acceleration and deceleration.

Due to the demand of providing a reasonable validation of the LHeC final design a Flexible Momentum Compaction (FMC) cell based lattice has been adopted. Specifications require isochronicity, path length controllability, large energy acceptance, small higher-order aberrations and tunability. An example layout, which fulfils these conditions, is shown in Fig. 14 and represents the lowest energy arc optics as example. It includes a two-step achromatic spreader and a mirror symmetric combiner to direct the beam into the arc. The vertical dispersion introduced by the first step bend is suppressed by the quadrupoles located appropriately between the two stages. The switchyards separate all 3 arcs into a 90 cm high vertical stack; the highest energy arc is not elevated and remains at the linac-level. A horizontal dogleg, used for path length adjustment and made of 3 - 13 cm long dipoles, is placed downstream of each spreader providing a tunability of ±1 cm (10° of RF).

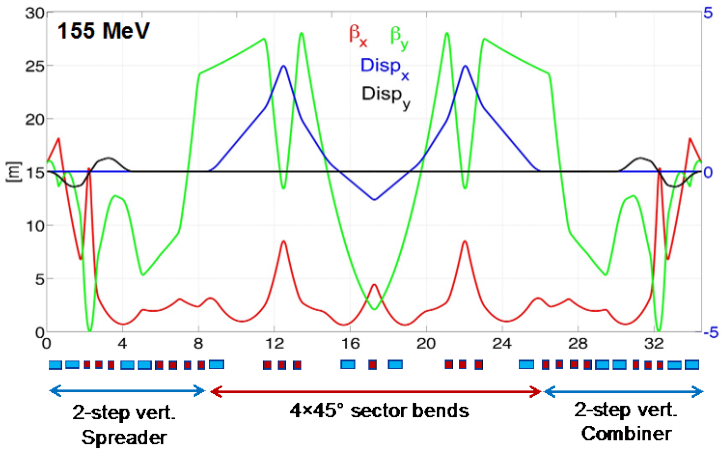

Figure 14: Optics based on the FMC cell for the lowest energy return arc. Horizontal (red curve) and vertical (green curve) beta-function amplitudes are illustrated. Blue and black curves show, respectively, the evolution of the horizontal and vertical dispersion.

The recirculating arc at 155 MeV is composed of 4 - 70 cm long dipoles to bend the beam by 180° and of a series of quadrupoles (two triplets and one singlet). A complete first-order layout for switchyards, arcs and linac-to-arc matching sections has been accomplished for all the arcs. Injection into the racetrack at 5MeV is accomplished through a rectangular chicane, configured with four identical rectangular bends and 11 quadrupoles distributed in a mirror symmetric fashion, leaving six independent quadrupole gradients to control: betas and alphas at the beginning of the linac (4 parameters), momentum compaction (1 parameter) and the horizontal dispersion (1 parameter). The chicane optics features a horizontal achromat, by design, with tunable momentum compaction to facilitate bunch-length control and finally with Twiss functions matched to the specific values required by the linac.

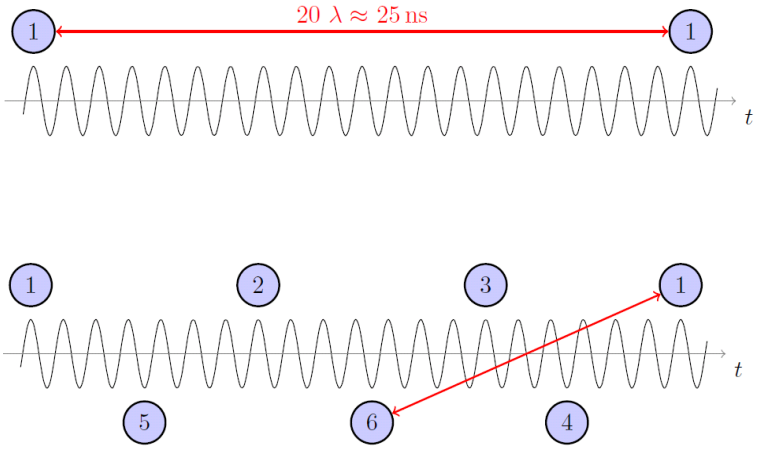

Figure 15: (Top) Basic RF structure, without recirculation with bunches injected every 25 ns. (Bottom) When the recirculation is in place, both linacs are populated with bunches at different turns. Presented recombination pattern maximizes the separation between the two low energy bunches (at the first and sixth turn).

The path length of each pass is chosen to be precisely an integer number of RF wavelengths except for the highest energy pass whose length is shifted by half an RF wavelength to recover the energy through deceleration. In order to minimize collective effects, the number of RF wavelengths that determines the arc's lengths has been tuned to avoid different bunches in the same bucket, like it would happen with a full turn length equal to an integer number of 20 λ. The lattice is therefore adjusted to achieve nearly constant bunch spacing. Special care has been taken to select a pattern that maximizes the distance between the lowest energy bunches circulating into the machine at the first and last turn (bunches 1 and 6 in Fig. 15). This comes from the fact that, with a nearly constant β function, the kicks from HOMs are more disruptive at lower rigidities, thus if two low energy bunches follow each other, the Beam Break Up (BBU) threshold current can be reduced. Fig. 16 is obtained following a test bunch in its path from the injector to the dump. The energy profile shows that the arcs' lengths are properly tuned to obtain the maximum acceleration and deceleration.

The total beam path for a full 3 pass accelerating cycle is around 300 m leading to an approximate footprint of 43m × 16m of the ERL itself.

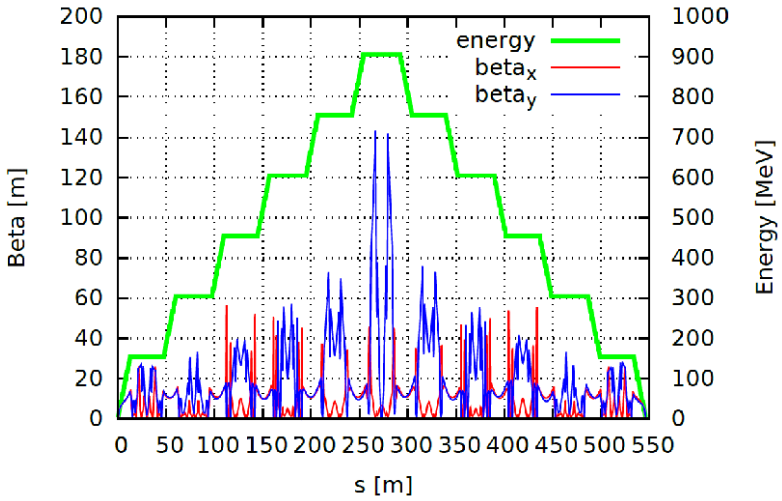

Figure 16: Energy and Twiss parameter tracked for the whole lattice.

In conclusion, the case for PERLE is quite compelling; it will serve as a unique 'testbed' for demonstrating validity of innovative beam dynamics solutions proposed for the LHeC. In particular, scaling of energy recovery to a large-scale SRF installation raises concerns about multi-pass BBU, an instability that has previously been seen and studied in detail in the Jefferson Lab FEL [12]. There are still open questions about scaling of instability thresholds to higher beam energies and a large-scale SRF installation [13] that could be addressed at PERLE. We propose PERLE to experimentally address these challenges with unique new additional accelerator capability. The facility would enable experimental exploration of multiple-passes and high current operation.

4.3.5 **Summary and Outlook**

Here, we discussed novel approach to meet the LHeC challenges of adding new accelerator capabilities (ERL with multiple-passes, tens of GeV at high current, tens of mA). They were addressed through exploration of innovative lattice solutions. Effective implementation of Energy Recovering Linac technology requires: proper design of multi-pass optics, fine control of beam stability and losses (halo), preservation of 6D bunch quality, energy recovery efficiency, multiple-beam diagnostic devices, and development of ERL-specific commissioning and optics tuning procedures[14, 15].

Scaling of energy recovery to multi-GeV energies also encounters incoherent synchrotron radiation energy loss and spread, which asymmetrize accelerated and decelerated beam energies and profiles. These asymmetries substantially complicate multi-pass energy recovery and matching, and ultimately they limit the energy reach of the ERL due to recirculating arc momentum acceptance. Scaling of energy recovery to a large-scale SRF installation also raises concerns about multi-pass BBU. We propose PERLE to experimentally address these issues as well.

Presented unique design of the IR optics gives the impression that luminosity of 10^{34} $cm^{-2}s^{-1}$ is within reach.

4.3.6 References

1. D. Pellegrini, A. Latina, D. Schulte, S.A. Bogacz, “Beam-dynamics driven design of the LHeC energy-recovery linac”, PRSTAB (2015).
2. D. Pellegrini, “Beam Dynamics Studies in Recirculating Machines”, Ph.D. Thesis, EPFL, Switzerland, 2016.
3. O. Brüning et al, “DEVELOPMENT OF AN ERL BASED TEV ENERGY EP AND EA COLLIDER AT CERN” ICFA Beam Dynamics Newsletter No 68, December 2015.
4. J. Rosenzweig and L. Serafini, “Transverse particle motion in radio-frequency linear accelerators”, Phys. Rev. E, vol. 49, Feb 1994.
5. 12 GeV CEBAF Upgrade, Reference Design, www.jlab.org/12GeV
6. J. L. Abelleira Fernandez *et al.* (LHeC Study Group), “A Large Hadron Collider at CERN”, J. Phys. G. 39 (2012) 075001.
7. B. Parker, presentation in the LHeC Workshop, Chavannes-de-Bogis, 2015, https://indico.cern.ch/event/356714/.
8. S. Fartoukh, “Achromatic telescopic squeezing scheme and application to the LHC and its luminosity upgrade”, Phys. Rev. ST Accel. Beams 16, 111002 (2013).
9. R.Tomás, in the Meeting on LHeC with Daresbury group, Daresbury, UK, 2012, https://indico.cern.ch/event/207665/.
10. M. Korostelev, E. Cruz-Alaniz, D. Newton, A. Wolski, O. Brüning, and R. Tomás, “LHeC IR optics design integrated into the HL_LHC lattice”, in Proceedings of the 4th International Particle Accelerator Conference, Shanghai, China, 2013, MOPWO063.
11. E. Cruz-Alaniz, D. Newton, R. Tomás and M. Korostelev, “Design of the Large Hadron Electron collider interaction region”, Phys. Rev. ST Accel. Beams 18, 111001 (2015).
12. S.A. Bogacz, A. Hutton et al., “CEBAF-ER Experiment Proposal", Je_erson Lab, PAC22 proposal PR-02-102, June 2002.
13. G. Hoffstaetter and I. Bazarov, “Beam-breakup Instability Theory for Energy Recovery Linacs", in Phys. Rev. ST Accel. Beams, 7, p. 054401, 2004.
14. ICFA Beam Dynamics Newsletter on ERL Technology, No. 68, Eds. J. Wang and W. Chou, Dec. 2015.

15. T. Powers and C. Tennant, “Implications of Incomplete Energy Recovery in SRF-Based Energy Recovery Linacs", in Proc. of ERL'07, Daresbury, UK, p. 75.

16. PERLE, Conceptual Design Report, 2015, unpublished

4.4 Lattice Design for Super Proton Proton Collider (SPPC)

Feng Su, Jie Gao, Yukai Chen, Jingyu Tang, Dou Wang,

Yiwei Wang, Sha Bai, Tianjian Bian, Dengjie Xiao

Mail to: sufeng@ihep.ac.cn

Institute of High Energy Physics, Chinese Academy of Sciences, Beijing, China

4.4.1 Introduction

With the discovery of the Higgs boson at the LHC, the world high-energy physics community is investigating the feasibility of a Higgs Factory as a complement to the LHC for studying the Higgs and pushing the high energy frontier. CERN physicists are busy planning the LHC upgrade program, including HL-LHC and HE-LHC. They also plan a more inspiring program called FCC, including FCC-ee and FCC-hh. Both the HE-LHC and the FCC-hh are proton-proton (pp) colliders aiming to explore the high energy frontier and expecting to find new physics [1, 2, 3]. Chinese accelerator physicists also plan to design an ambitious machine called CEPC-SPPC (Circular Electron Positron Collider-Super Proton Proton Collider). The CEPC-SPPC program contains two stages. The first stage is an electron-positron collider with center-of-mass energy 240 GeV to study the Higgs properties carefully. The second stage is a proton-proton collider at center-of-mass energy of more than 70 TeV [4]. The SPPC design is just starting, and first we developed a systematic method of how to make an appropriate parameter choice for a circular pp collider by using an analytical expression of beam-beam tune shift, starting from the required luminosity goal, beam energy, physical constraints at the interaction point (IP) and some technical limitations [5, 6]. Then we start the lattice design according to the parameter list and have the first version SPPC lattice.

4.4.2 SPPC Parameter Choice

The energy design goal of the SPPC is about 70-100 TeV, using the same tunnel as the CEPC, which is about 59 km in circumference [7, 8, 10]. A larger circumference for the SPPC, like 100 km, is also being considered. It is planned to use superconducting magnets of about 20 T [4]. We obtain a set of parameters for the 59.2 km SPPC. In this set of parameters, the full crossing angle θc keeps the separation of 12 RMS beam sizes for the parasitic crossings. The luminosity reduction factor due to the crossing angle is larger than 0.9 and the ratio of β^* and σ_z is about 15. We also give a set of parameters for the larger circumference SPPC, considering both 80 km and 100 km. Table 1 is the parameter list for the SPPC. We choose the dipole field as 20 T and get a center-of-mass energy of 70 TeV. If we want to explore the higher energy, we should make the